Highlights of Spanish Astrophysics XII, Proceedings of the XVI Scientific Meeting of the Spanish Astronomical Society held on July 15 - 19, 2024, in Granada, Spain. M. Manteiga, F. González Galindo, A. Labiano Ortega, M. Martínez González, N. Rea, M. Romero Gómez, A. Ulla Miguel, G. Yepes, C. Rodríguez López, A. Gómez García and C. Dafonte (eds.), 2025

VLA observations of the pre-transitional disk HD 169142

Placinta-Mitrea, F.[1], **Osorio, M.**[1], **Anglada, G.**[1], **Gómez, J. F.**[1], **Blázquez-Calero, G.**[1], **Fuller, G. A.**[2,3], **Macías, E.**[4], **Carrasco-González, C.**[5], **Torrelles, J. M.**[6], **Rodríguez, L. F.**[5]

[1] Instituto de Astrofísica de Andalucía (CSIC), Glorieta de la Astronomía S/N, E-18008 Granada, Spain
[2] Jodrell Bank Centre for Astrophysics, Department of Physics and Astronomy, The University of Manchester, Oxford Road, Manchester M13 9PL, UK
[3] I. Physikalisches Institut, University of Cologne, Zülpicher Str. 77, 50937 Köln, Germany
[4] European Southern Observatory (ESO), Garching bei München, Germany
[5] Instituto de Radioastronomía y Astrofísica UNAM, Apartado Postal 3-72 (Xangari), 58089 Morelia, Michoacán, Mexico
[6] Institut de Ciències de l'Espai (CSIC) and Institut de Ciències del Cosmos (UB)/IEEC, Can Magrans S/N, Cerdanyola del Vallès (Barcelona), Spain

Abstract

We present preliminary results of a multi-wavelength Very Large Array study at 7 mm, 9 mm, and 2 cm of the HD 169142 pre-transition disk.

1 Introduction

Some disks around young stars show a central cavity (and, in some cases, additional annular gaps) in their dust emission. This substructure is believed to result from the interaction with the disk of one or more still-forming planets, and is therefore considered a sign of the onset of the planetary formation process. These disks appear to be at an intermediate stage between full disks, where planet formation is not yet evident, and debris disks, where most of the disk material has dispersed or become planets, and are therefore called "transitional disks" ([4]). A subfamily of transitional disks are the so-called "pre-transitional disks", which present a residual inner disk inside the cavity ([5]).

HD 169142 is an intermediate-mass Herbig Ae/Be star (1.49 $M_\odot$; [7]) located at a distance of 114 pc [16]. The star is associated with a pre-transitional disk of dust with a central cavity, which is surrounded by a sequence of rings and gaps ([14, 6, 11, 16]). The inner, brightest ring is located at a radius of ∼25 au, while three additional, weaker rings are located at radii ∼57-76 au ([16]). A central cm/mm source, interpreted as a possible residual disk or a free-free radio jet, is found inside the cavity ([11, 16]). Also, two IR protoplanet candidates have been identified inside the cavity and the first gap ([17, 3, 8]), being HD 169142 the first case where a protoplanet candidate with Keplerian motion has been found [8]. This makes HD 169142, along with the PDS 70 system [9], one of the most compelling cases where protoplanets have been detected by direct imaging.

The source has been extensively observed at wavelengths shorter than ∼1 mm with the Atacama Large Millimeter/submillimeter Array (ALMA) (e.g., [6, 16, 10]). However, in order to probe the brightest regions, where the dust emission at ∼1 mm becomes optically thick, observations at longer wavelengths are more suitable. In this work we present a summary of the results obtained by [15] from Karl G. Jansky Very Large Array (VLA) observations at 7 mm, 9 mm, and 2 cm. At these wavelengths, the dust emission is optically thinner and better traces the true surface density distribution in the inner ring, as well as possible variations in the spectral index, which might be related to dust grain evolution. The observed emission traces preferably particles with sizes of the order of the observing wavelength and, thus, 7 mm VLA observations are better suited to trace particles that have reached pebble sizes in their process to form planetary bodies, while VLA observations at cm wavelengths can identify the presence of ionized gas.

2 Observations

Observations in Bands Q (7 mm), Ka (9 mm), and Ku (2 cm) were carried out along 10 observing sessions, from 4 March to 23 April 2018, using the VLA in its A configuration (see Table 1 and [15]). The amplitude, bandpass and delay calibration was made using 3C 286, whereas the complex gain calibration was performed by observing J1745−2900 (Sgr A*) at 7 mm and J1820−2528 at 9 mm and 2 cm.

The observation of HD 169142 with the VLA is hampered by its low declination, resulting in the source being observed at low elevations and on short tracks, yielding an elongated beam in the north-south direction and poorer phase stability, especially at the highest frequencies. In order to improve the phase calibration (at the cost of decreasing the on-source time), the 7 mm observations were performed with the fast-switching technique.

Data reduction and calibration were carried out with the package Common Astronomy Software Applications (CASA) version 6.2.1-7 [13]). Each scheduling block was processed separately through the VLA calibration pipeline and the calibrated sets were inspected and further flagging was applied when it was necessary. Once the calibration was completed for each scheduling block, all the 7 mm blocks were concatenated with the CASA task `concat`, obtaining a single *uv* data set with a higher signal to noise ratio.

Finally, deconvolved images were obtained with CASA task `tclean`. Because of the low declination of the source, the synthesized beam in the natural-weighting maps is very elongated in the north-south direction, resulting in somewhat distorted images. In order to obtain a better signal-to-noise ratio for extended structures (rings) as well as higher fidelity images,

Table 1: Log of VLA observations

Band	Frequency (GHz)	Wavelength (mm)	Date	Time on source (min)
Q	43.9	7	04 Mar 2018	40
	43.9	7	09 Mar 2018	40
	43.9	7	30 Mar 2018	40
	43.9	7	01 Apr 2018	40
	43.9	7	10 Apr 2018	19
	43.9	7	19 Apr 2018	40
	43.9	7	22 Apr 2018	40
	43.9	7	23 Apr 2018	40
Ka	33	9	05 Apr 2018	103
Ku	15	20	05 Mar 2018	33

uv tapering was applied to the data to enlarge the beams in the direction of the minor axis, and thus make them rounder. Also, to enhance the signal-to-noise, azimuthally averaged radial intensity profiles were obtained. The resulting maps and intensity profiles are shown in Figures 1, 2, and 3.

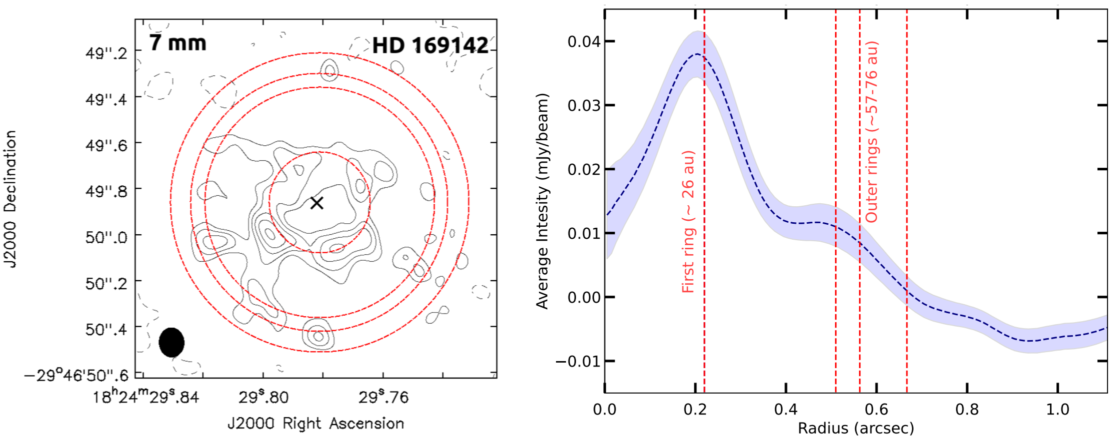

Figure 1: Left: Map of HD 169142 at 7 mm, obtained with natural weighting and a uvtaper of 1500 kλ to emphasize the extended emission and get a rounder beam. The synthesized beam is $0.128'' \times 0.108''$ (PA=2.9°) and the contour levels are −2, 2, 3, 4, 5, and 6 times the rms noise of 11.5 μJy beam^{-1}. The cross indicates the position of the star, and the red circles the positions of the rings obtained from a fit to the 1.3 mm ALMA image of [16]. Right panel: Azimuthally averaged radial intensity profile at 7 mm. The light blue shaded area represents the uncertainty estimated from the rms of the map. (Figure adapted from [15])

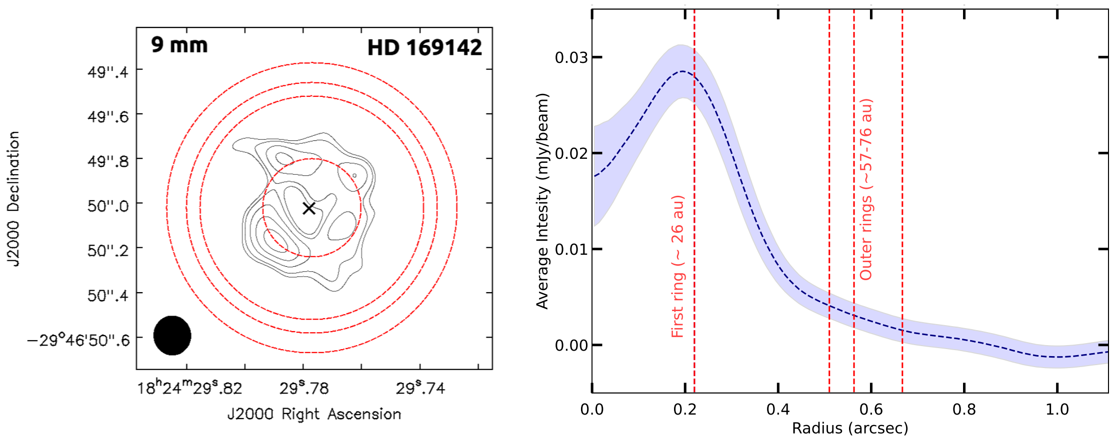

Figure 2: Same as Figure 1, but for the 9 mm data. The synthesized beam is $0.176'' \times 0.166''$ (PA=3.9°) and the contour levels are −2.5, 2.5, 3, 4, 5, and 6 times the rms noise of 8.5 μJy beam^{-1}. (Figure adapted from [15])

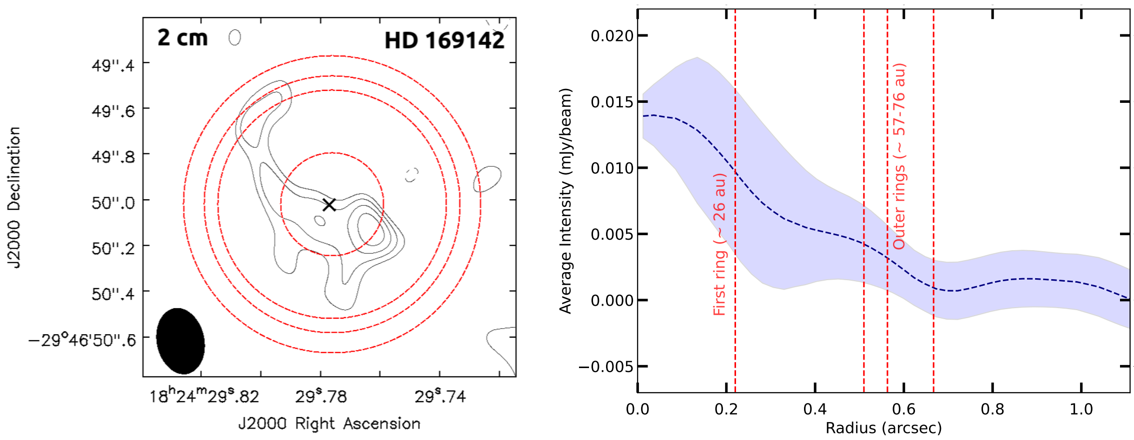

Figure 3: Same as Figure 1, but for the 2 cm data. The synthesized beam is $0.29'' \times 0.20''$ (PA=11.7°) and the contour levels are −2.5, 2.5, 3, 3.5, and 4 times the rms noise of 5.0 μJy beam^{-1}. (Figure adapted from [15])

3 Results and discussion

Figure 1 (left panel) shows the Q-band (7 mm) image of HD 169142. The map clearly shows the first ring and the central cavity in the dust emission of this transitional disk, with a hint of the emission of the outer rings. This is better illustrated in the radial profile shown in the right panel of Figure 1. There is no clear detection of emission associated with the central source, first reported at 7 mm by [11], which is also detected as a weak source in the 1.3 mm ALMA image of [16]. Table 2 lists the measured flux densities at epoch 2018.3 ([15]) for the different components of the disk. We note that the total flux density at 7 mm in the 2018.3

observations is 1.16 ± 0.13 mJy, which is about half the value of 2.0 ± 0.4 obtained by [11] (epochs = 2013.8 - 2014.3) with a similar setup, suggesting a significant decrease in the flux density of the dust emission of the disk by a factor of ∼1.7 in a time interval of ∼4 years. There is also a decrease in the flux density of the central source, which was detected by [11] with a flux density of 74 ± 15 μJy, but remains undetected, with an upper limit of < 35 μJy, in the 2018.3 observations. According to the results obtained by [11], the central compact source appears to have a different nature, as it has a spectral index $\alpha = 0.82 \pm 0.17$, which is significantly flatter than the expected spectral index from dust emission ($\alpha \geq 2$), suggesting that its nature is free-free emission from an ionized radio jet (e.g., [2]).

Table 2: Flux densities and spectral indices

Component	$S_\nu(7\,\mathrm{mm})$ (mJy)	$S_\nu(9\,\mathrm{mm})$ (mJy)	$S_\nu(2\,\mathrm{cm})$ (mJy)	$\alpha_{7\mathrm{mm}-9\mathrm{mm}}$	$\alpha_{9\mathrm{mm}-2\mathrm{cm}}$
Central region	<0.035[a]	<0.025[a]	0.014 ± 0.005	...	...
First ring	0.62 ± 0.05	0.30 ± 0.05	0.044 ± 0.012	2.54 ± 0.65	1.61 ± 0.27
Outer rings	0.32 ± 0.09	0.080 ± 0.040	0.034 ± 0.016	5.23 ± 2.16	0.72 ± 0.58
Total	1.16 ± 0.13	0.46 ± 0.07	0.112 ± 0.024	3.24 ± 0.66	1.18 ± 0.13

[a] 3-σ upper limit.

Figure 2 shows the Ka-band (9 mm) image and radial intensity profile of HD 169142. The first ring of the disk and its cavity are clearly detected, both in the map and in the radial profile. There are hints of emission from the central source and the outer rings, but no clear detection is achieved in either case. Table 2 lists the measured flux densities. Similarly to what happens with the data at 7 mm, the emission at 9 mm also shows a decrease with respect to the previously observed emission. The total flux density measured at 9 mm in the 2018.3 observations ([15]) is 0.46 ± 0.07 mJy, while the flux density measured in 2014.2 by [11] was 0.85 ± 0.15 mJy, which is a factor ∼1.8 smaller, similar to the decrease observed at 7 mm. The spectral index from 7 to 9 mm obtained from the 2018.3 data (Table 2 and [15]) is $\alpha_{7\mathrm{mm}-9\mathrm{mm}} = 3.24 \pm 0.60$, which is similar to the value of $\alpha_{7\mathrm{mm}-9\mathrm{mm}} = 3.0 \pm 0.7$ than can be inferred from the flux densities reported by [11]. Thus, both results consistently indicate that the emission detected in the 7-9 mm range is dominated by thermal dust emission ($\alpha > 2$); this dust emission originates mainly from the first ring, located at a distance of ∼ 25 au from the star, and shows signs of variability on time scales of a few years (see [15] for more details).

The emission at 9 mm from the central source has also decreased between 2014 and 2018, as it was detected by [11] with a flux density of 45 ± 14 μJy in 2014, but is not detected, with a 3-σ upper limit of 0.025 mJy, in the 2018 observations.

Finally, Figure 3 shows the Ku-band (2 cm) image and radial intensity profile of HD 169142. The source is detected, for the first time at 2 cm, but the image is noisy and the shape of the emission is not well defined. This, together with the large size of the beam, makes it difficult to establish where the dominant emission is coming from. In both the map and the radial intensity profile it is difficult to discriminate which fraction of the emission may originate from the central source and which from the disk rings. For this reason, the values of the parameters of the separate components listed in Table 2 should be taken with caution, since they have large uncertainties. Nevertheless, the total flux value is more reliable, since it has a better signal to noise ratio. Using the total flux at 2 cm, together with the value at 9 mm, a spectral index $\alpha_{9\mathrm{mm}-2\mathrm{cm}} = 1.18 \pm 0.13$ is obtained, which is well below the expected minimum value for dust emission ($\alpha_{\mathrm{dust}} > 2$), thus suggesting that the emission at 2 cm has a significant free-free contribution from ionized material with a flatter spectral index ($-0.1 \leq \alpha_{\mathrm{free-free}} \leq 2$), likely from the central source. This is consistent with the results of [11], who estimated the spectral index of the central source and concluded that it was dominated by free-free emission, probably from a radio jet (e.g.,[2, 18]).

Acknowledgments

G.A., J.F.G., G.A.F., M.O., and F.P-M are supported by grants PID2020-114461GB-I00, PID2023-146295NB-I00, and CEX2021-001131-S, funded by MCIN/AEI /10.13039/501100011033. F.P.-M. also acknowledges support by the predoctoral grant PRE2021-100926, funded by MCIN/AEI/ 10.13039/ 501100011033. The National Radio Astronomy Observatory is a facility of the National Science Foundation operated under cooperative agreement by Associated Universities, Inc. This work was presented at the symposium "On the origin of stars and their planets: A holistic view" within the framework of the XVI Scientific Meeting of the Spanish Astronomical Society.

References

[1] Andrews, S. M., Huang, J., Pérez, L. M., et al. 2018, ApJL, 869, L41

[2] Anglada, G., Rodríguez, L. F., & Carrasco-González, C. 2018, A&ARv, 26, 3

[3] Biller, B. A., Males, J., Rodigas, T., et al. 2014, ApJL, 792, L22

[4] Calvet, N., D'Alessio, P., Watson, D. M., et al. 2005, ApJL, 630, L185

[5] Espaillat, C., Calvet, N., D'Alessio, P., et al. 2007, ApJL, 670, L135

[6] Fedele, D., Carney, M., Hogerheijde, M. R., et al. 2017, A&A, 600, A72

[7] Garg, H., Pinte, C., Hammond, I., et al. 2022, MNRAS, 517, 5942

[8] Hammond, I., Christiaens, V., Price, D. J., et al. 2023, MNRAS, 522, L51

[9] Keppler, M., Benisty, M., Müller, A., et al. 2018, A&A, 617, A44

[10] Leemker, M., Booth, A. S., van Dishoeck, E. F., et al. 2022, A&A 663, A23

[11] Macías, E., Anglada, G., Osorio, M., et al. 2017, ApJ, 838, 97

[12] Macías, E., Espaillat, C. C., Osorio, M., et al. 2019, ApJ, 881, 159

[13] McMullin, J. P. et al., 2007, Astronomical Data Analysis Software and Systems XVI, 376

[14] Osorio, M., Anglada, G., Carrasco-González, C., et al. 2014, ApJL, 791, L36

[15] Placinta-Mitrea, F., et al. 2024, in preparation

[16] Pérez, S., Casassus, S., Baruteau, C., et al. 2019, AJ, 158, 15

[17] Reggiani, M., Quanz, S. P., Meyer, M. R., et al. 2014, ApJL, 792, L23

[18] Rodríguez, L. F., Zapata, L. A., Dzib, S. A., et al. 2014, ApJL, 793, L21